P-wave velocity inversion from prestack seismic data using FO-CDS traveltime approximation with higher order coherence measures

Felipe A. V. Pena, Marcelo J. L. Mesquita and João C. R. Cruz, UFPA, Brazil

This paper was prepared for presentation during the 18th International Congress of the Brazilian Geophysical Society, held in Rio de Janeiro, Brazil, October 16-19, 2023.

Abstract

A good estimated velocity model is fundamental for coherent seismic imaging, which is essential for defining exploration targets in geological interpretation. We find in the geophysical literature several methods to obtain a data consistent velocity model using seismic wave propagation traveltimes. Most of them, for example, traveltime tomography, use as input the picked traveltimes on pre-stack seismic data, which is a computationally exhaustive step and sometimes creates erroneous information. In this paper, we propose an inversion algorithm based on the finite offset common diffraction surface (FO-CDS) traveltime approximation. The FO CDS inversion method aims to obtain accurate velocity models in the depth domain with a low computational effort, being adequate for obtaining seismic images or as an initial model for more sophisticated inversion methods, like Full Waveform Inversion. To reach higher performance, we use an objective function based on high order coherence measures. For comparison, we applied the FO CDS inversion to synthetic data using two objective functions, i.e. the conventional semblance and also the modified fourth-order semblance version in order, to verify the best result of the estimated velocity model. In conclusion, we have the FO-CDS inversion using the modified fourth-order semblance provided a better estimate of the searched-for parameters during the inversion process.

Introduction

An accurate velocity macro-model is essential for seismic reflection imaging. The most commonly used method in seismic exploration is the velocity analysis (Dix, 1955). The estimation of velocity macro-models remains a crucial topic for theoretical research. In addition, the difficulty in this theme is based on two points: (1) the underdetermination of the problem, which implies that the velocity macro-model that focuses the events reflected in depth in the correct positions can only be recovered with the introduction of a priori information, such as well data, and (2) the strong non-linearity that links the traces in the seismogram to the velocity macro-model(Farra and Madariaga, 1988) .

The seismic tomography (Bishop et al., 1985; Farra and Madariaga, 1988) is the most commonly used inversion method. This approach describes the model as a layered set with interval velocity and smooth interfaces, and the data consists of selected traveltimes for specific events. The block model is optimized by fitting the calculated traveltimes to the selected traveltimes. In reflection tomography, the underdetermination of the problem appears through the velocity-depth ambiguity (Williamson, 1990; Stork, 1992a,b; Tieman, 1994). The process of picking the traveltime from prestack data is complex and laborious, as the chosen events have to be identified in all traces and interpreted as a reflector in the model. In addition, instabilities may arise in the optimization procedure for complex models (Chapman, 1985; Amand and Virieux, 1995).

Stereotomography was introduced as a different approach to tomographic inversion. In this algorithm, the horizontal component of slowness (tilt) information concerning the source and receiver is used with the traveltime for selected locally coherent reflection events in the prestacked data (Billette and Lambare, 1998; Billette et al., 2003).A smooth distribution of velocities and parameters associated with the reflection/diffraction points is sought globally and iteratively during the inversion process.

Other methods use traveltime information as kinematic attributes of the wavefield related to the hypothetical waves obtained from stacking the Zero-Offset (ZO) Common Reflection Surface (CRS) (Müller, 1999; Jäger, 1999) into several domains. Normal Incidence Point (NIP)Tomography is one such example (Duveneck, 2004). Zhang et al. (2001) proposed an extension of the ZO CRS method, the so-called finite-offset (FO) CRS method. Unlike the ZO CRS, the 2D FO CRS automatically estimates five kinematic parameters for each selected reference traveltime in the prestack data domain. Like the ZO CRS, the FO CRS is a hyperbolic traveltime approximation. Unlike the ZO CRS, the FO CRS uses an arbitrary FO central ray as a reference. This means that it is capable of locally approximating the traveltime at far-offset positions within a certain range (Garabito et al., 2011). Later on, Soleimani and Balarostaghi (2016) created a new method called finite offset common diffraction surface(FO-CDS) stack to overcome the problem of conflicting dips on FO CRS stack and remove some geological interpretation ambiguities in the seismic section. Some modifications were done to improve the CDS stack operator, with the idea of partial common reflection surface stack to enhance the seismic image quality. Garabito et al. (2017) also used the FO-CDS operator to enhance and regularize seismic data.

This paper presents an inversion approach based on the P-wave velocity inversion methodology presented by Mesquita et al. (2018), which is constituted of two steps. In the first step, we use as input data an initial velocity

model obtained by Dix's formula and the picked traveltimes from a time migrated section, and by using the image ray technique we find the reflective interfaces in the depth of the model. In the second step, the in depth generated velocity model is used as input, where the parameterization of the velocity model is done layer by layer. To obtain the convergence of the objective function around a global maximum, we applied the Very Fast Simulated Annealing (VFSA) optimization method described by Ingber (1989). This work aims to apply the inversion method based on the FO-CDS traveltime approximation for synthetic data by comparing two different objective functions, one using conventional second-order semblance and another with modified fourth-order semblance, to evaluate the best result of the inversion process.

CDS hyperbolic traveltime approximation.

Zhang et al. (2001) developed the hyperbolic traveltime approximation for paraxial rays around the central ray that considers a finite offset between sources and receivers. In Figure 1, we see a central ray that starts from S, reflects in a reflector R in the subsurface, and emerges on the surface in G. When a point R on the subsurface is considered a diffraction point, the Huygens Principle states that this point becomes a new secondary wavefront source as soon as the incident wavefront arrives at R. This diffraction point generates a new wavefront propagating upward along the central ray to emerge at G. Using the equation 1, we can construct the stacking surface of Figure 1 that provides a traveltime approximation based on kinematic wavefield attributes. Because this operator is associated with the central diffracted ray, it is called the Common Diffraction Surface at finite offset (FO-CDS).

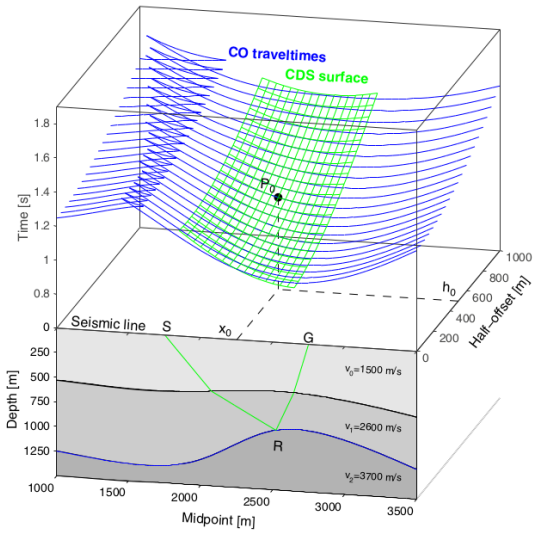

Figure 1: At the bottom, we have a model of two layers over a half-space, where the central ray with half-offset h_0 and midpoint x_0 are shown in green. At the top we have curves in blue which are the traveltimes for common-offset gather, and in green, the times of the FO-CDS operator associated with point P_0 (modified from Garabito et al. 2011).

$$t^2(\Delta x_m,\Delta h)=\left[t_0+\left(\frac{sen\beta_G}{v_G}+\frac{sen\beta_s}{v_s}\right)\Delta x_m+\left(\frac{sen\beta_G}{v_G}-\frac{sen\beta_s}{v_s}\right)\Delta h\right]^2$$
$$+t_0\left[K_3\frac{cos^2\beta_G}{v_G}-K_2\frac{cos^2\beta_S}{V_S}\right]\Delta x_m^2+t_0\left[K_3\frac{cos^2\beta_G}{v_G}-K_2\frac{cos^2\beta_S}{v_S}\right]\Delta h^2$$
$$+2t_0\left[K_3\frac{cos^2\beta_G}{v_G}+K_2\frac{cos^2\beta_S}{v_S}\right]\Delta x_m\Delta h. \qquad (1)$$

where t_0 is the traveltime along the central ray, β_S and β_G are the departure and emergence angles of the central ray at the positions of the sources and the receivers, with coordinates x_S and x_G. The midpoint displacement is described by $\Delta x_m = x_m - x_0$ and the half offset displacement by $\Delta h = h - h_0$, where $x_0 = (x_G + x_S)/2$ is the midpoint and $h_0 = (x_G - x_S)/2$ is the half offset from the central ray. The midpoint x_m and half offset h are the coordinates of an arbitrary paraxial ray. The P-wave velocity at the source and receiver locations is described by v_S and v_G, respectively. The variables K_2 and K_3 are the curvatures of the hypothetic wavefronts associated with the central ray and starting at the scattering point in the depth, calculated at their respective emergence points.

Coherence measures

For all midpoints and reflectors, we can compute the total coherence measure over the traveltimes calculated by the FO-CDS approximation. The higher the coherence value, the better the considered interpretation model. For many traces, we can fall back on the fact that when stacking multiple channels simultaneously, the resulting amplitude is usually greatest where the individual channels are similar (or coherent), i.e., they are stacked in phase. Following the same reasoning, the resulting amplitude is smaller when the signals are incoherent. Furthermore, the main objective of the inversion is to find a model where this measure is maximum.

One of the measures of coherence adopted will be the semblance function (Neidell and Taner, 1971), which is used to estimate the presence or absence of correlated signals along traveltime curves calculated by the FO-CDS method. The conventional second order semblance function (S), which belongs to the interval $0 \le S(\mathbf{p}) \le 1$ and which is the measure between the energy of the signal after stacking traces and the energy of all the seismic traces involved in the summation, is calculated by

$$S_2(\mathbf{p}) = \frac{\sum_{k=-w}^{w}\left[\sum_{i}^{N} u_i(t_k)\right]^2}{N\sum_{k=-w}^{w}\left[\sum_{i=1}^{N} u_i(t_k)^2\right]} \qquad (2)$$

Where the FO-CDS attributes are $\mathbf{p}$=($\mathbf{v}$,$\mathbf{z}$($\mathbf{v}$),$\mathbf{q}$($\mathbf{v}$,$\mathbf{z}$)), with $\mathbf{q}$=(K_2,K_3,β_S,β_G), u_i corresponds to the amplitude of the ith trace in double time $t(i)$, with $i = 1,...,N$ that lies along the hyperbolic stacking path FO-CDS defined by the parameters $\mathbf{p}$, the value N is the number of dashes in the CMP family data, the external summation means that the stacking is performed in a temporal window of width $2w+1$, which is related to the waveform of the event, defined about the trajectory of the central stacking.

A general expression can be obtained to calculate semblance coherence through the expression

$$S_m = 1 - \frac{\sum_{k=-w}^{w}\left[\sum_{i=1}^{N}(u_{ik}-\mu_1)^m\right]}{\sum_{k=-w}^{w}\left[\sum_{i=1}^{N}u_{ik}^m\right]} \quad (3)$$

where $u_{ik} = u_i(t_k)$ and μ_1 is the arithmetic mean for the set of amplitudes along the FO-CDS traveltime curve.

For comparison purposes, a modification proposed by Mesquita and Cruz (2021) in the semblance coherence measure was also tested, in which we used the median instead of the mean of the equation 3.

$$\check{S}_m = 1 - \frac{\sum_{k=-w}^{w}\left[\sum_{i=1}^{N}(u_{ik}-M)^m\right]}{\sum_{k=-w}^{w}\left[\sum_{i=1}^{N}u_{ik}^m\right]} \quad (4)$$

where M is the median for the amplitudes along the FO-CDS traveltime curve. The median is calculated as follows

$$M = \begin{cases} u_{(N+1)/2}, & \text{N is odd} \\ u_{\frac{N}{2}} + u_{\frac{N}{2}+1}, & \text{N is even.} \end{cases} \quad (5)$$

In the inversion process, the arithmetic mean of the calculated semblance values is used as a maximization parameter for each layer. Thus, the equations 3 and 4 become:

$$E = -\left[\frac{1}{n}\sum_{j=1}^{n}(S_m)_j\right] \quad (6)$$

$$\check{E} = -\left[\frac{1}{n}\sum_{j=1}^{n}(\check{S}_m)_j\right] \quad (7)$$

where n is the number of analyzed CMPs, the nature of the VFSA optimization algorithm is to calculate the minimum value of energy, so it is usual to multiply E by the factor (-1) so that its maximum value is estimated.

Inversion algorithm

The algorithm adopted in this work is exemplified in Figure 2, where the main points will be presented below:

1) the first step consists of obtaining the a priori information that will be used in the inversion, that is, the traveltimes obtained by picking a migrated section.

2) Time to depth conversion using image rays from a first-guess velocity model. This model can be estimated from the time interval velocities after applying Dix's formula (Dix, 1955).

3) After generating an initial depth velocity model, this step performs ray tracing and calculation of the wavefield parameters to estimate the traveltimes by the hyperbolic operator FO-CDS.

4) Measure the semblance coherence between the estimated and actual events (using pre-stacked data). If the coherence measure is maximum, the velocity model in depth is accepted, the estimated model is fixed for the layer, and the process is repeated for the next layer; otherwise, the process restarts from step two with an updated velocity model following the VFSA logic.

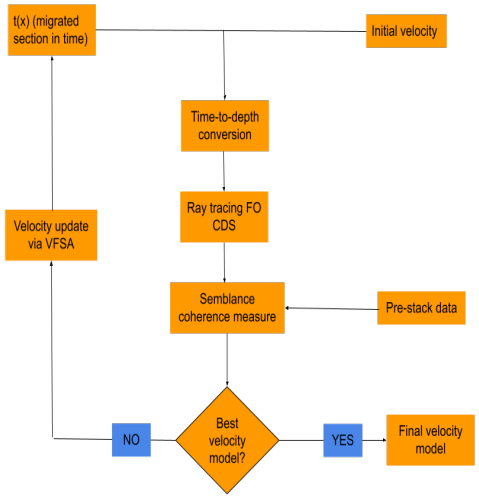

Figure 2: Inversion strategy flowchart.

We compare two measures of coherence, and they are the second-order conventional semblance shown in the equation 3 and the fourth-order modified semblance observed in the equation 4.

Results

Two-layers model

The inversion algorithm was tested on a simple two-layer model shown in Figure 3 at three different noise levels defined by the equation below

$$S_s = S_e + \left(\frac{1}{sr}\right)\left(\frac{\sqrt{2A}S_m}{2A}\right)N, \quad (8)$$

where S_s is the output signal, S_e is the input signal, S_r is the signal-to-noise ratio, which in this case were $S_r = 50$, $S_r = 30$ and $S_r = 10$. S_m is the absolute value of the maximum signal, A is the energy per sample, and N is the noise probability distribution (Gaussian). The Figure 4 is section CMP 300 with the $S_r = 10$ as an example.

In the tests of the inversion strategy, nine CMPs were analyzed for each layer, starting from CMP 60 to CMP 380 at 40 (1000 m) intervals. Each of these CMPs contains 30 traces, with an interval of 50 m between them and a maximum opening of 1450 m to the right or left. The first CMP (CMP 60) is located at 737.5 m, and the last is at 8737.5 m. The parameters used for the inversion process for the synthetic data are in Table 1. A velocity search interval was defined with a margin of 200 m/s above and below the correct velocity for the model. The smallest velocity value of the seek range was adopted as the initial velocity.

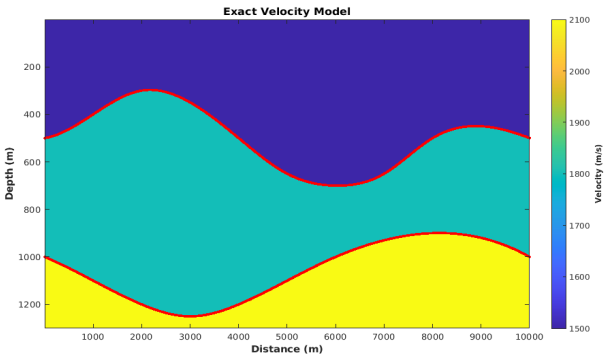

Figure 3: Exact velocity model. This line in red characterizes the model's real interfaces.

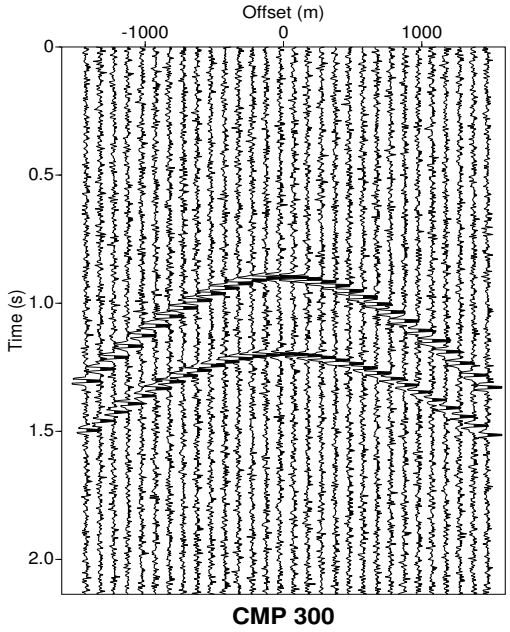

Figure 4: CMP 300 with a signal-to-noise ratio of 10.

Table 1: Table with the input parameters for the simple model inversion process. These data were used in booth strategies.

Input parameters for the inversion.		
Magnitude	Layer 1	Layer 2
Exact speed $[v(m/s)]$	1500	1800
Initial velocity $[v_0(m/s)]$	1300	1600
Velocity search range $[v_{ib}(m/s)]$	1300-1700	1600-1900
Initial temperature (T_0)	2.0	2.0
Cooling rate (c)	0.1	0.2

After the ten tests, each with 500 iterations, the results were obtained in the tables 2 and 3. The averages of the ten velocities reached for each one of the layers (v_{avg1} and v_{avg2}), the percentage error of these averages about the exact velocity of the layer (ev_{avg1} and ev_{avg2}), the average of mean squared errors for each of the interfaces (ez_{avg1} and ez_{avg2}), and the interval between the maximum and minimum semblance achieved for each layer (ΔE_1 and ΔE_2), the smaller this difference, the better the convergence of the proposed method.

Table 2: Results of the inversion processes for the conventional second-order semblance case for three different noise levels.

Results obtained			
Parameter	$S_r = 50$	$S_r = 30$	$S_r = 10$
$v_{avg1}(m/s)$	1514,31	1517,68	1513,71
$v_{avg2}(m/s)$	1880,58	1819,52	1514,13
$ev_{avg1}(\%)$	0,9117	1,1788	0,9421
$ev_{avg2}(\%)$	4,4767	1,0844	1,8240
$ez_{avg1}(m)$	19,0757	20,0561	18,9046
$ez_{avg2}(m)$	36,2809	18,8686	19,4531
ΔE_1	0,000237	0,002392	0
ΔE_2	0,012408	0,003513	0,009370

Table 3: Results of the inversion processes for the modified fourth-order semblance case for three different noise levels.

Results obtained			
Parameter	$S_r = 50$	$S_r = 30$	$S_r = 10$
$v_{avg1}(m/s)$	1518,55	1519,78	1513,19
$v_{avg2}(m/s)$	1868,27	1860,97	1513,05
$ev_{avg1}(\%)$	1,2246	1,2142	0,8706
$ev_{avg2}(\%)$	3,7929	1,0844	1,7895
$ez_{avg1}(m)$	20,3116	20,6750	18,7569
$ez_{avg2}(m)$	36,3526	31,5518	20,2341
ΔE_1	0,006026	0	0,003004
ΔE_2	0,044084	0,014970	0,010291

According to the tables 2 and 3 presented, it can be noted that the algorithm that used the modified fourth-order semblance obtained a better estimate of the parameters involved in the inversion in some cases, in the first layer, the estimates were better in the case of $S_r = 10$, that is when the signal-to-noise ratio was low. In the second layer, the estimates regarding the velocities were better when the modified fourth-order semblance was used than the conventional second-order semblance.

Multi-layers model

The multi-layer model was built and processed using the Seismic Unix (SU) open-source package. The acquisition was simulated with the beam theory, considering the synthetic model of Figure 5. This model consists of five homogeneous layers with velocities $v_1 = 1507m/s$, $v_2 = 1700m/s$, $v_3 = 1900m/s$, $v_4 = 2100m/s$ and $v_5 = 2300m/s$. The geological model acquisition parameters are in the table 4.

18 CMPs are analyzed in this test, from CMP 60 to CMP 400; these have maximum coverage, in this case, 30 traces. The first CMP (CMP 60) is located at 737.5 m, and the last CMP (CMP 400) at 9237.5 m.

Conventional second-order semblance

The table 5 presents the magnitudes used in the inversion process where v is the exact velocity, v_0 is the starting

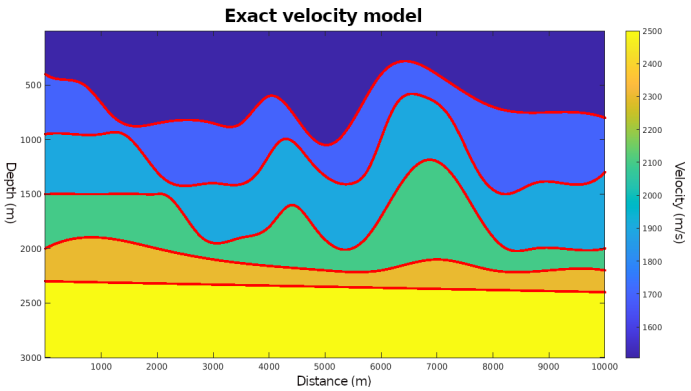

Figure 5: Geological model of constant seismic velocities. The red lines represent the exact positions of the interfaces in the model.

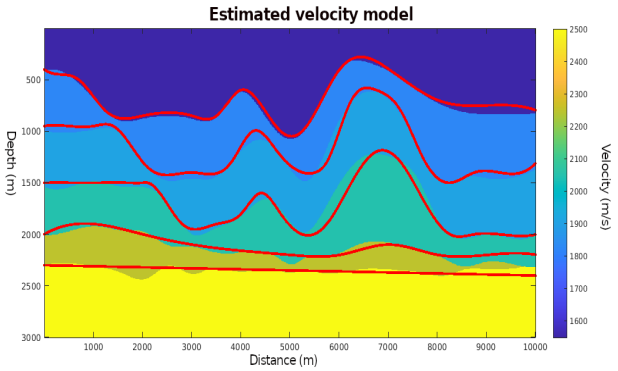

Figure 6: Velocity model estimated using the conventional second-order semblance as objective function.

Table 4: Table with parameters for acquiring the multi-layer model.

Acquisition parameters	
Number of shots	200
Distance between sources	50 m
Number geophones	60
Distance between geophone	50 m
Arrange	Split-spread
Spread	-1475-25 25 1475 m
Number of samples in time	1001
Interval between samples	4 ms

velocity, v_{ib} is the velocity search interval. T_0 and c, which are the initial temperature and cooling rate, are functions linked to the VFSA optimization method. They were chosen empirically and maintained for all tests to compare different tested semblances. The main results obtained at the end of the process are the objective function E, the estimated speed v_e, the percentage error of the estimated velocity about the exact velocity e_v, and the mean squared error of the interfaces e_z calculated by the equation:

$$e_z = \sqrt{\frac{1}{n-1}\sum_{i=1}^{n}(z - z_e)^2}, \tag{9}$$

where, z is the exact depth and z_e is the estimated depth.

Table 5: Table with the parameters and results of the multi-layer model inversion process using the second-order semblance coherence measure.

Input parameters and obtained results.					
Parameter	Layer 1	Layer 2	Layer 3	Layer 4	Layer 5
$v(m/s)$	1507	1700	1900	2100	2300
$v_0(m/s)$	1900	1607	2221	1900	2100
$v_{ib}(m/s)$	1400-2000	1500-1900	1700-2100	1900-2300	2100-2500
T_0	2,0	2,0	2,0	2,0	2,0
c	0,2	0,2	0,2	0,2	0,3
E	0.3542	0.1185	0.2950	0.3734	0.4059
$v_e(m/s)$	1547	1821	1906	2047	2247
$e_v(\%)$	3,1920	7,1176	0,3368	2,5238	2,2898
$e_z(m)$	39,60	48,51	64,13	50,81	40,67

After 100 iterations for each layer, the velocity model could be estimated (Figure 6). It can be observed from table 5 that the estimated results agree satisfactorily with the exact model, except for the velocity of layer 2, which is not well estimated.

Modified fourth-order Semblance

In this test, the inversion process was performed using another measure of coherence, which in this case was the modified fourth-order. Table 6 shows the input parameters and results of the inversion process for this case. It can be seen that the modified fourth-order coherence measure obtained better velocity estimates for almost all layers. It is interesting to note the case of the second layer, which in the test that uses the semblance of order coherence measure, presented an error of $e_v = 7.11\%$ while, in the inversion that used the fourth order coherence measure modified order estimated a velocity with a relative error of only $e_v = 3.19\%$, less than half of the previous case.

Table 6: Table with the parameters and results of the inversion process of model multi-layer using the modified fourth-order semblance coherence measure.

Input parameters and obtained results.					
Parameter	Layer 1	Layer 2	Layer 3	Layer 4	Layer 5
$v(m/s)$	1507	1700	1900	2100	2300
$v_0(m/s)$	1300	1500	1700	1900	2100
$v_{ib}(m/s)$	1300-1700	1600-2000	1700-2100	2100-2500	2300-2700
T_0	2,0	2,0	2,0	2,0	2,0
c	0,2	0,2	0,2	0,2	0,3
E	0.3526	0.1012	0.3627	0.0589	0.5930
$v_e(m/s)$	1532	1754	1914	2096	2319
$e_v(\%)$	2,1511	3,1972	0,7368	0,1448	0,8260
$e_z(m)$	33,74	41,60	67,18	64,56	46,84

As in the previous test, the input velocity models are based on previously estimated layers and the initial velocity of the layer to be estimated. After 100 iterations for the five layers, the inversion process estimated the velocity model seen in Figure 7.

Conclusion

In general, it was observed that the proposed inversion algorithm based on the FO-CDS traveltime approximation is efficient in estimating the velocity model. The proposed method managed to estimate velocity models consistent with the data, thus being able to be used for in-depth imaging.

For the tests of the inversion algorithm carried out with different degrees of signal-to-noise ratio, the version with the modified fourth-order semblance as an objective function obtained a better estimate of the parameters for the case of a low signal-to-noise ratio. In other cases, the conventional second-order semblance method presents an

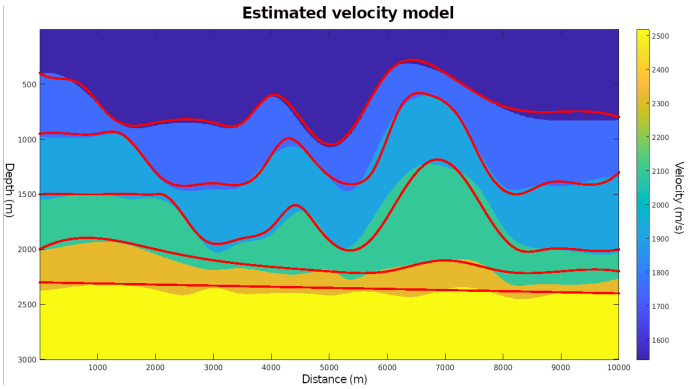

Figure 7: Velocity model estimated using the modified fourth-order semblance as objective function.

advantage in the estimated parameters.

We can observe that the estimated velocity parameters and interfaces by the inversion method were close to the exact values. Therefore, it is recommended to test this algorithm for more complex synthetic models and real data. As the method requires a low computational effort, it can be used to estimate initial velocity models for application in more sophisticated methods of inversion techniques, such as FWI, and in applying prestacking migration techniques.

Acknowledgments

The authors would like to thank the Brazilian institutions UFPA (*Universidade Federal do Pará*), PETROBRAS (*Petróleo Brasileiro S/A*) for the research support. The thanks are also extended to CAPES for the scholarship.

References

Amand, P., and Virieux, J., 1995, Nonlinear inversion of synthetic seismic-reflection data by simulated annealing: 65th Annual SEG Meeting and Exposition,Expanded Abstracts, **58**, 612–615.

Billette, F., and Lambare, G., 1998, Velocity macro-model estimation from seismic reflection data by stereotomography: Geophys. J. Int., **137**, 671–690.

Billette, F., Le Begat, S., Podvin, P., and Lambare, G., 2003, Practical aspects and applications of 2d stereotomography: Geophysics, **63**, 1008–1021.

Bishop, T., Bube, K., Cutler, R., Langan, R., Love, P., Resnick, J., Shuey, R., and Spinder, D., 1985, Tomographic determination of velocity and depth in laterally varying media: Geophysics, **50**, 903–923.

Chapman, C., 1985, Ray theory and its extensions: Wkbj and maslov seismogram: Geophysical Journal, **58**, 27–43.

Dix, C., 1955, Seismic velocities from surface measurements: Geophysics, **20**, 68 – 86.

Duveneck, E., 2004, Tomographic determination of seismic velocity models with kinematic wavefield attributes: Ph.D. thesis, Karlsruhe University, Karlsruhe.

Farra, V., and Madariaga, R., 1988, Non-linear reflection tomography: Geophysical Journal, **95**, 135–147.

Garabito, G., Oliva, P., and Cruz, J., 2011, Numerical analysis of the finite offset common reflection surface traveltime approximations: Journal of Applied Geophysics, **74**, 89–99.

Garabito, G., Cruz, J., Oliva, P., and Sollner, W., 2017, Seismic data enhancement and regularization using finite offset common diffraction surface (cds) stack: Journal of Applied Geophysics, **136**, 80–90.

Ingber, L., 1989, Very fast simulated reannealing: Mathematical and Computer Modelling, **12**, no. 8, 967–993.

Jäger, R., 1999, The common-reflection-surface stack: Master's thesis, Karlsruhe University, Karlsruhe.

Mesquita, M. J. L., and Cruz, J. C., 2021, Analysis of an alternative semblance function applied to finite-offset common-reflection-surface tomography: Congress of the Brazilian Geophysical Society.

Mesquita, M. J. L., Cruz, J. C., and Garabito, G., 2018, Velocity inversion by global optimization using finite-offset common-reflection-surface stacking applied to synthetic and tacutu basin seismic data: Geophysics, **84**, no. 2, 1–55.

Müller, T., 1999, The common reflection surface stack method-seismic imaging without explicit knowledge of the velocity model: Ph.D. thesis, Karlsruhe University, Karlsruhe.

Neidell, N. S., and Taner, M. T., 1971, Semblance and other coherency measures for multichannel data: Geophysics, **36**, 482–497.

Soleimani, M., and Balarostaghi, M., 2016, Seismic image enhancement in post stack depth migration by finite offset cds stack method: J. Petrol. Explor. Prod. Technol., **6**, 605–6015.

Stork, C., 1992a, Singular value decomposition of the velocity reflector depth tradeoff, part 1: Introduction using a two-parameter model: Geophysics, **57**, 927–932.

Stork, C., 1992b, Singular value decomposition of the velocity reflector depth tradeoff, part 2: High resolution analysis of a generic model: Geophysics, **57**, 933–943.

Tieman, H., 1994, Investigating the velocity depth ambiguity of reflection traveltimes: Geophysics, **59**, 1763–1773.

Williamson, P., 1990, Tomographic inversion in reflection seismology: Geophysical Journal International, **100**, 255–274.

Zhang, Y., Bergler, S., and TygelM., H. P., 2001, Common-reflection-surface (crs) stack for common-offset.: Geophys. Prospect., **49**, 709–718.